NASA TECHNICAL MEMORANDUM

NASA TM-78892

NASA TM-78892

(NASA-TM-78892) INVESTIGATION OF THE EFFECT OF CERAMIC COATINGS ON ROCKET THRUST CHAMBER LIFE (NASA) 26 p HC A03/MF A01 CSCL 21H

N78-26173

Unclas
G3/20 23337

INVESTIGATION OF THE EFFECT OF CERAMIC COATINGS ON ROCKET THRUST CHAMBER LIFE

by R. J. Quentmeyer, H. J. Kasper, and J. M. Kazaroff
Lewis Research Center
Cleveland, Ohio 44135

TECHNICAL PAPER to be presented at the
Fourteenth Propulsion Conference
cosponsored by the American Institute of Aeronautics
and Astronautics and the Society of Automotive Engineers
Las Vegas, Nevada, July 25-27, 1978

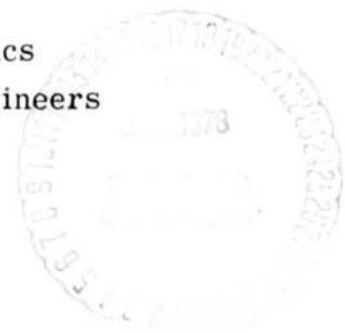

INVESTIGATION OF THE EFFECT OF CERAMIC COATINGS ON ROCKET THRUST CHAMBER LIFE

by R. J. Quentmeyer, H. J. Kasper, and J. M. Kazaroff

National Aeronautics and Space Administration
Lewis Research Center
Cleveland, Ohio 44135

E-9630

Abstract

Two cylindrical rocket thrust chamber cylinders were coated with a 0.203 mm (0.008 in.) layer of zirconium-oxide using a process that employed electrodeposition of metal to a spray coated mandrel. The cylinders were cyclically tested using hydrogen-oxygen propellants at a nominal chamber pressure of 4.14 MN/m^2 (600 psia) to show the effect of the coating on life. Both cylinders failed prematurely due to causes unrelated to the coatings. One cylinder failed at 80 cycles because of a defective weld and the other failed at 659 cycles because of a blocked cooling passage. Post destructive analysis showed no cooling passage wall deformation. Where erosion of the coating occurred, the coating thickness stabilized at 0.061 mm (0.0024 in.) within 80 cycles and remained well adhered throughout the tests. The hot-gas-side metal wall temperature and the theoretical maximum effective strain were reduced by 80 and 92 percent, respectively, where the coating was 0.203 mm (0.008 in.) thick and by 40 and 50 percent, respectively, where the coating was 0.061 mm (0.0024 in.) thick compared to an uncoated cylinder. The 50 and 92 percent reductions in maximum effective strain resulted in theoretical lives of 1900 cycles and greater than 10 000 cycles, respectively, compared to 300 cycles for the uncoated cylinder.

Introduction

The current generation of high performance, reusable rocket engines such as the Space Shuttle Main Engine (SSME) and the Advanced Space Engine (ASE) which is a 89 kN (20 000 lbf) thrust technology development engine, are designed to operate at high chamber pressure to reduce the engine size and weight. However, high chamber pressure, coupled with extended reuse requirements, impose very difficult cooling requirements on the thrust chamber, particularly at the throat region. To meet the cooling and life requirements, the inner wall of these reusable thrust chambers are fabricated with relatively high strength, high conductivity, copper base alloys. This allows a wall thickness sufficient to carry the cooling pressure and thrust loads, while maintaining reasonable wall temperatures and coolant pressure drop.

However, as thrust chamber size is reduced, by increasing chamber pressure for a given thrust level, a cooling limit will eventually be reached for conventional regenerative cooling; that is, there will not be sufficient cooling pressure drop available to maintain the wall temperature within its maximum operating limit and the thrust chamber life will be severely reduced. The SSME and ASE appear to be near the threshold of the cooling limit for reusable, regeneratively cooled thrust chambers cooled by liquid hydrogen.

Presently, these high pressure thrust chambers are life limited due to the high plastic strain levels encountered in the hot-gas-side wall during each thermal cycle. This high strain is caused by the large hot-gas-side wall to outer surface (backside) wall temperature difference that exists during the burn portion of the cycle. This repeated large plastic strain appears to promote progressive thinning of the cooling passage wall at the centerline until the wall thins to the point where it can no longer sustain the pressure load. This phenomenon has been observed by several investigators.[1-3] Therefore, if the present trend toward higher chamber pressure continues for reusable thrust chambers, cooling schemes other than purely regenerative cooling will have to be used to reduce the high thermal strain in the thrust chamber wall.

One way to reduce the thermal strain is to use a thermal barrier, such as a ceramic coating, on the hot-gas-side wall to reduce the large wall temperature difference. The use of ceramic coatings as an effective thermal barrier on rocket thrust chambers is not a new concept. It has been previously explored by many investigators.[4-10] The major drawback to the use of coatings is their tendency to spall or flake off during repeated thermal cycles. This is due to the large difference in thermal coefficient of expansion between the coating material and the metal wall and the low ductility of the ceramic coating. One method of improving adhesion of the coating to the metal wall is to apply multiple layers, or graded coatings having various degrees of ductility. The objective is to have the layer which is applied to the metal wall high in metal content and to have the layer exposed to the hot combustion gases pure ceramic.

The most widely used method of applying ceramic coatings is by spraying them onto the thrust chamber wall with an arc plasma spraying gun. Another method is to spray the coating onto a mandrel and electroform the thrust chamber liner to the coating.[11] This reversed process should provide an improved ceramic-metal bond because the metal is electrodeposited to a relatively rough ceramic surface.

Since the current trend is to attempt to design high pressure thrust chambers which can endure hundreds of thermal cycles, further investigation was warranted into the use of ceramic coatings which have the potential of providing very long thrust chamber life.

In light of this, an experimental investigation was initiated at the Lewis Research Center to study the effect of ceramic coatings on thrust chamber life. The objectives were to: (1) evaluate the effectiveness of a zirconium-oxide coating applied to a thrust chamber wall by the electroforming process; (2) show the reduction in strain achieved by use of the coating; and (3) relate the results to thrust chamber life.

The test apparatus used to perform this investigation was the cylindrical thrust chamber

STAR Category 20
AIAA 78-1034

assembly, previously used in the low cycle fatigue investigation reported in reference 1. Two cylinders, fabricated from electrodeposited copper, and coated on the inner cylindrical wall with zirconium-oxide, were made for the test program. The cylinders were cyclically tested at a chamber pressure of 4.14 MN/m^2 (600 psia). The results of post destructive, thermal, and structural analyses are presented. These results are compared with the results obtained from reference 1 for an uncoated copper cylinder tested at the same conditions.

Apparatus and Test Procedure

Cylindrical Thrust Chamber Assembly

Figure 1 shows a schematic of the cylindrical thrust chamber assembly. The thrust chamber consisted of an annular injector, a liquid hydrogen-cooled outer cylinder, which served as the test section, and a water-cooled centerbody, which formed the annular thrust chamber throat. The thrust chamber had a contraction and expansion area ratio of 1.79. At a chamber pressure of 4.14 MN/m^2 (600 psia) the thrust was approximately 5.34 kN (1200 lbf). Gaseous hydrogen and liquid oxygen were used as propellants. The cylindrical test section was separately cooled with liquid hydrogen, which was disposed of by a burn-off stack. The cooling water for the centerbody was dumped at the thrust chamber exit.

Cylindrical Test Section

The cylindrical test sections were 15.24 cm (6.0 in.) in length and had an inside diameter of 6.60 cm (2.6 in.). The ceramic coated cylinders were fabricated by a technique similar to that reported in reference 11. The fabrication process, as shown in figure 2, was started with a 6.60-cm (2.6-in.) diameter steel mandrel. The mandrel was arc plasma sprayed with a layer of zirconium-oxide. This was followed by an arc plasma sprayed Nichrome coating to provide an electrically conductive surface for the electroforming process. The total thickness of the zirconium-oxide-Nichrome coating was 0.203 mm (0.008 in.) with the Nichrome coating accounting for approximately 0.0127 mm (0.0005 in.) of this thickness. The mandrel assembly was then placed in a copper sulfate plating bath where it was continuously rotated during the plating operation. After a sufficient layer of copper was plated to the assembly, the copper wall was machined to the proper diameter and 72 constant area cooling channels, 0.169 cm (0.0665 in.) wide and 0.127 cm (0.05 in.) high, were milled into the copper layer. The cooling channel wall was 0.089 cm (0.035 in.) thick and the ribs were 0.129 cm (0.051 in.) wide. After machining, the cooling channels were filled with wax and a copper closeout electrodeposited to the backside. The wax was then melted out of the cooling channels and the mandrel was pressed out of the assembly. Final machining was performed and the manifolds added. This method of fabrication produced a smooth, even, zirconium-oxide surface having a surface finish of 2 microns (80 μin.) rms. Figure 3 shows a cross-section of the cylinder wall with the cooling channel dimensions. The uncoated copper cylinder had the same geometric configuration as the coated cylinder. The copper cylinder was fabricated by machining a liner from a forged copper billet. The rest of the fabrication process was the same as that for the coated cylinders. The cylinders were designed to be separately cooled with liquid hydrogen at a nominal flow rate of 0.91 (kg/sec (2.0 lbm/sec).

Instrumentation

The instrumentation consisted primarily of Chromel/Constantan backside wall and rib thermocouples. The backside wall thermocouples were located at four circumferential locations 90^o apart at the throat plane. There were two additional backside thermocouples, one 1.49 cm (0.586 in.) upstream of the throat plane and one 1.27 cm (0.50 in.) downstream of the throat plane. The junctions of the backside thermocouples were peened into small holes drilled into the backside surface. Four rib thermocouples were located at the throat plane of each cylinder. Two thermocouples were located 0.089 cm (0.035 in.) from the interface of the coating and copper wall and two were located 0.178 cm (0.070 in.) from the interface of the coating and copper wall. One cylinder also had eight additional rib thermocouples, four located 1.49 cm (0.586 in.) upstream and four located 1.27 cm (0.50 in.) downstream of the throat plane to obtain an axial thermal profile. Details of the thermocouple locations are shown in figure 3. The rib thermocouples were the same as those described in reference 2. Each thermocouple consisted of a Chromel and Constantan wire 0.025 mm (0.001 in.) in diameter inside a sheath made of 0.356 mm (0.014 in.) stainless steel tubing. The junction was made in a ball of silver solder which was plated with 0.005 mm (0.0002 in.) of gold. The probe was then spring loaded against the bottom of the rib hole. Figure 4 shows a coated cylinder with all of the thermocouples installed. The liquid hydrogen inlet temperature was measured by a platinum resistance bridge transducer inserted in the inlet manifold. The hydrogen outlet temperature was measured by a Chromel/Constantan thermocouple inserted in the outlet manifold.

Injector

Figure 5 shows the thrust chamber injector. Gaseous hydrogen and liquid oxygen were used as propellants. Liquid oxygen was injected through 70 showerhead tubes arranged in two circular rows, 36 in the inner row and 34 in the outer row. The tubes were made of 0.23 cm (0.091 in.) o.d. stainless steel having a 0.03 cm (0.012 in.) thick wall. Two chamber pressure taps were located in the outer row of oxidizer tubes. The gaseous hydrogen was injected entirely through the porous Regimesh face plate. The face plate was removable, so that it could be replaced if damaged. Injector uniformity tests were performed with ablative chambers and the uniformity was found to be satisfactory. Characteristic exhaust velocity efficiency ranged from 93 to 96 percent.

Centerbody

Figure 6 shows the thrust chamber centerbody. The centerbody was fabricated by machining 40 rectangular cooling channels into the outer periphery of a contoured copper alloy forging. The cooling channels were closed out by electrodepositing copper to the outer surface and then machining the

surface to the final contour. The centerbody had a 4.06 cm (1.6 in.) o.d. in the combustion zone and a 5.33 cm (2.1 in.) o.d. at the throat and was 15.24 cm (6.0 in.) in length. The expansion half-angle was 7.5°. The centerbody was inserted through the center of the injector and bolted into place from the back side.

A 0.076 to 0.127 mm (0.003 to 0.005 in.) zirconium-oxide flame sprayed coating was applied to the outside surface to reduce the heat load and prolong the centerbody life. The centerbody was cooled with a nominal water flow of 5.44 kg/sec (12 lbm/sec). The water entered the centerbody behind the injector, passed through the cooling channels and was dumped at the thrust chamber exit.

Test Facility

The tests were conducted at the Lewis Research Center rocket engine test facility. This is a 222 410 N (50 000 lbf) sea-level rocket test stand equipped with an exhaust-gas muffler and scrubber. The facility used pressurized propellant storage tanks to supply the propellants and coolants to the thrust chamber. Figure 7 is a schematic of the test facility showing the propellant and coolant supplies and the instrumentation. The liquid hydrogen used to cool the cylinder was disposed of through a burn-off stack. The thrust chamber exhaust gas and the centerbody water coolant were expelled into the scrubber. Due to the small volume of the thrust chamber combustion zone, an external igniter was used to back-light the combustion chamber. The igniter used gaseous oxygen and gaseous hydrogen as propellants. The ignition source was a high voltage spark.

Data Recording

All pressures and temperatures were recorded in digital form on a magnetic tape for entry into a digital computer. The digital recording system was set at a basic sampling rate of 2500 words per second. After processing, all of the data and calculations performed on the data could be printed out on the control room terminal at 0.1 second intervals.

Test Procedure

The cycle chosen for the tests was one where the heat-up portion of the cycle was long enough for the hot-gas-side wall temperature to reach steady-state, and where the cool-down portion of the cycle was long enough to bring the entire cylinder back to liquid hydrogen temperature. The cycle to achieve this condition was 3.5 seconds in duration, 1.7 seconds from ignition to the end of the combustion portion of the cycle, and 1.8 seconds to bring the cylinder back to liquid hydrogen temperature. The liquid hydrogen coolant was continuously flowed throughout a cyclic test, however, the weight flow varied from its initial rate as a function of the heat load to the cylindrical test section. Figure 8 is a display from a computer plotting routine of chamber pressure and liquid hydrogen-coolant weight flow showing how the liquid hydrogen weight flow varied with the heating cycle. During the first cycle of any given test a liquid hydrogen precool was used to bring the entire cylinder to liquid hydrogen temperature before ignition of the thrust chamber propellants. Short tests, consisting of just two cycles, were made with each new cylinder to establish the desired test condition. After the desired test conditions were achieved, the thrust chamber was continuously cycled until the supply of liquid hydrogen was nearly depleted. Generally, 70 to 90 cycles could be achieved on one tank of liquid hydrogen.

A solid state timer, accurate and repeatable to ±0.0001 second was used to program the test events. Fuel and oxidizer flows were controlled by initially setting fixed valve positions which would nominally set chamber pressure and mixture ratio. After the nominal chamber pressure was reached, both chamber pressure and mixture ratio were adjusted to the desired condition by a controller. The liquid hydrogen coolant weight flow and pressure were set by a combination of tank pressure, and upstream and downstream valve positions. The centerbody water flow was set to its maximum rate by pressurizing the water tank to a pressure of 10.34 MN/m^2 (1500 psia).

The tests were monitored by a closed-circuit television camera and a test cell microphone. The TV and audio outputs were recorded on magnetic tape for playback. Figure 9 shows the cylindrical thrust chamber during the combustion portion of a cyclic test. The cylinders were inspected after each test series to observe the condition of the coating.

Test Results

Table I gives a summary of the test results. Both zirconium-oxide coated cylinders failed prematurely, but not due to failure of the coating. Cylinder S/N 36 failed after only 80 cycles due to a flaw in a manifold weld seam near the injector. The failure caused unrepairable damage and the testing was terminated. Cylinder S/N 37 had a burnout failure in the throat region due to a blocked cooling passage. However, the fact that this cylinder endured 659 cycles of testing before failure emphasized the significant effect that coatings can have on prolonging thrust chamber life. Cylinder S/N 34 developed a crack in the throat plane at 210 cycles and was typical of the failure mechanism encountered in the high strain environment of these types of thrust chambers.

Post Destructive Analysis

After the testing was completed, each cylinder was subjected to a post test destructive analysis. The cylinders were sectioned to determine the amount of deformation in the cooling passage wall and to measure the coating thickness.

Both coated cylinders showed an erosion of the coating surface, but not uniformly over the entire surface. Figure 10 shows the region of cylinder S/N 36 where the coating remained completely intact. Figure 11 shows another view of cylinder S/N 36 showing the eroded areas of the coating. The throat plane in this figure is the cross section plane that contains the thermocouple hole centerlines. Approximately 55 percent of the coating remained completely intact in the throat region.

Figure 12 shows the burnout area in the throat region of cylinder S/N 37. During the destructive analysis, the cylinder was cut so that a cross section of the cooling passage in which the burnout occurred could be examined. It was found that the cooling passage was completely blocked with plater's wax at two locations. Consequently, the only cooling provided to this passage was due to the heat conduction through the copper liner to the adjacent cooling passages. Figure 13 shows the plater's wax in the cooling passage. It was concluded that the hot spot caused the cooling passage wall to locally and progressively deform during the cyclic testing until the coating could no longer adhere to the copper wall. Once this local area was exposed to the hot gas, a burnout occurred on the 659th cycle.

Cylinder S/N 37 showed erosion in the throat region similar to cylinder S/N 36. However, due to the greater number of cycles experienced by cylinder S/N 37, only about 30 percent of the original coating surface remained intact as compared to 55 percent for cylinder S/N 36. Figure 14 shows the uniformly eroded coating surface in the throat region of cylinder S/N 37. Excluding the burned out area of cylinder S/N 37, there was no other area on either cylinder where bare copper was exposed due to failure of the coating to adhere.

The measured rib temperatures showed that most of the erosion in both cylinders occurred during the initial 80 cycles of testing. This was evidenced by the observed rib temperatures in the areas where erosion occurred. Temperature data from a throat thermocouple in cylinder S/N 37 showed a continuous increase in steady-state temperature to about 80 cycles indicating the coating erosion was taking place. Beyond this, however, the steady-state temperature stabilized indicating that erosion was no longer occurring in that region as shown in figure 15. Although cylinder S/N 36 was tested for only 80 cycles the same characteristic of initial erosion was observed.

The coating thickness was measured in the stabilized eroded regions of both cylinders and was found to be a uniform 0.061 mm (0.0024 in.) including the thin Nichrome layer. The eroded coating in these areas appeared to be very well adhered, having a surface roughness of 8.6 to 9.7 microns (340 to 380 μin.) rms.

Figure 16 shows a cross section of cylinder S/N 37 at the throat plane at a circumferential location away from the burnout region. The coating at this location has eroded to the 0.061 mm (0.0024 in.) thickness. The uniformity of the coating can be seen in this figure. Note that there is virtually no deformation of the cooling passages, even after 659 thermal cycles. Compare this figure with the cross section of uncoated cylinder S/N 34 shown in figure 17, which developed a crack in the cooling passage wall at 210 cycles. The severely deformed cooling passages are typical of the failure mechanism reported in reference 1, that is, thinning of the cooling passage wall at the centerline until a rupture occurs. It was mentioned previously that cylinder S/N 37 failed prematurely due to a blocked cooling passage. However, if there had been no blocked cooling passage, one could conclude from figure 16 that the cylinder would have endured several hundred more cycles. The effectiveness of the coating in prolonging thrust chamber life can readily be seen from these two figures.

Thermal Analysis

One of the objectives of this program was to show the reduction in strain that could be achieved in the thrust chamber wall by use of a thermal barrier coating. In order to perform the necessary structural analysis, the cylinder cross-sectional temperature profile as a function of time was required.

The following procedure was used to generate the cylinder cross-sectional temperature profiles for the structural analyses: (1) the measured rib and backside temperatures were plotted as a function of time for each cylinder; (2) a thermal model of the cylinder wall cross section was developed; (3) the boundary conditions needed for the conduction analysis were calculated; and a two-dimensional conduction analysis was performed using the SINDA[12] thermal analyzer program until a best match of the experimental and theoretical rib and backside temperatures could be achieved.

Due to the large amount of data obtained in the experimental testing, a detailed analysis using the data from every cycle was not possible. However, random samples of all of the measured parameters were taken throughout the cyclic testing of each cylinder. Analysis of the data confirmed that once the desired cycle was established for a given cylinder, the test parameters remained essentially the same throughout the testing. Thus, it was concluded that any cycle was representative of a "nominal" cycle throughout the cylinder life.

Figure 18 shows the experimental rib and backside temperature data at the throat plane for the 203rd cycle of uncoated cylinder S/N 34. The temperatures from the rib thermocouples located 0.089 cm (0.035 in.) from the hot-gas-side wall were averaged. In like manner, the temperatures from the rib thermocouples located 0.178 cm (0.070 in.) in depth were averaged, and the temperatures from the four backside thermocouples were averaged. Also shown in this figure is the calculated match of the rib and backside temperature data and the thermal model used in the conduction analysis. Due to symmetry, only one-half of a cooling channel wall cross section was required for the model as shown in figure 3. The representative wall cross section was divided into 35 elements with a temperature node at the center of each element. In addition, there were surface nodes on each of the elements along the model boundaries. The relative locations of the thermocouples used to collect the experimental temperature data are also indicated in the figure. Input to the SINDA program requires the hot-gas-side and coolant-side boundary conditions as a function of time, so that a temperature profile can be generated as a function of time. The steady-state hot-gas-side heat transfer coefficient was obtained from unreported data using a calorimeter with the cylindrical thrust chamber configuration. The steady-state coolant side heat transfer coefficient was calculated from empirical correlations which best describe convective heat transfer to liquid hydrogen. In addition, the coolant-side heat transfer coefficient was varied around the cooling channel periphery to reflect the variation due to the different wall temperatures that exist around the periphery. The hot-

gas-side and the coolant-side heat transfer coefficients during the transients were not available from experimental data, therefore, as an initial input, they were assumed to vary from their steady-state values in proportion to variations in chamber pressure and liquid hydrogen weight flow for each time slice. Plots such as shown in figure 8 were used to make the adjustments in the heat transfer coefficients during the transients. This procedure did a reasonable job of fitting the temperature data, although minor adjustments were made in the boundary conditions, where needed, to best fit the data. The SINDA program is capable of performing a three-dimensional thermal analysis, but only a two-dimensional analysis at the throat plane of the thrust chamber was used for this work. The program outputs the temperature for each nodal point in the model, however, in figure 18 only the matching of the temperature data and the projected hot-gas-side wall temperature is shown. Using this technique, a cross-sectional temperature profile as a function of time could be generated for each cylinder.

It was assumed that the best projected hot-gas-side wall temperature was obtained when the calculated temperature data matched the experimental data of the thermocouple closest to the hot-gas wall. When this was done, a perfect match of the thermocouple data at the other two locations could not necessarily be achieved, as seen on figure 18. This was probably due to axial conduction effects not accounted for in this two-dimensional analysis.

Figure 19 shows the calculated matching of the rib and backside temperature data for cylinder S/N 37 at the fifth cycle, before any of the coating had eroded away. The rib and backside temperature data were averaged in the same manner as the data from cylinder S/N 34. The overshoot in the temperature data was caused by a slight overshoot in chamber pressure encountered in these tests. Note the large decrease in the calculated steady-state hot-gas-side metal wall temperature, T_{mw}, when compared to the uncoated cylinder. The metal wall temperature was reduced from 844 K (1520° R) for the uncoated cylinder to only 157 K (282° R) for the coated cylinder, a reduction of 80 percent. Although not shown on the figure, the calculated hot-gas-side ceramic wall temperature was 2922 K (5260° R), which is close to the melting temperature of zirconium-oxide. The steady-state metal wall to backside wall temperature difference, ΔT, and the heat flux, q, were also reduced 80 percent which shows how beneficial the coating is as a thermal barrier.

It was pointed out in the Post Destructive Analysis section that about 70 percent of the coating in the throat region of cylinder S/N 37 had eroded to a thickness of 0.061 mm (0.0024 in.). Two rib thermocouples at the two different depths and two backside thermocouples, all in the throat plane, were located in this region so that a thermal analysis of the cylinder wall in the eroded region could be made. Figure 20 shows the calculated matching of the experimental temperature data for the 576th cycle. The backside temperature data is the average of the two thermocouples which were in the eroded region. This analysis shows that the calculated T_{mw}, ΔT, and q were all reduced approximately 40 percent when compared to the uncoated cylinder. The calculated hot-gas-side ceramic wall temperature was 1878 K (3380° R). Thus, the eroded coating also provided a very effective thermal barrier. A summary of the thermal analysis is shown in Table II. The profound effect that the reduction in metal temperatures has on reducing the strain in the thrust chamber wall is described in the Structural Analysis section.

Structural Analysis

Life predictions of rocket thrust chambers have in the past been based on classical low cycle fatigue principles. These methods involved calculation of cyclic strain ranges which were used to enter laboratory generated isothermal life curves that related strain range and material cycles to failure. Experimental thrust chamber life tests have shown that the classical analytical methods do not necessarily apply to chamber life prediction.[1,2] The results of these tests have indicated that a reasonably accurate life prediction analysis must account for the cooling channel geometry change that results from channel wall thinning and bulging. Development of such a method is in progress but has not yet been completed. Therefore, in an attempt to present the life extending capabilities of coatings applied to rocket thrust chambers, the classical method has been used for this paper. Although the accuracy of this method for predicting actual cylinder life is questionable, it was felt that it was sufficiently accurate for analytically comparing the lives of coated and uncoated cylinders.

The structural analysis was performed with the aid of the BOPACE 3-D finite element computer program for three-dimensional analysis of problems in thermoviscoplasticity.[13] The program accounts for, in an incremental manner, effects of variable amplitude cyclic loads and temperatures. In addition, nonlinear variation of material properties with temperature, mechanically or thermally induced plasticity, and combinations of creep and stress relaxation are incorporated in the program.

Data from the Thermal Analysis section were used to define the thermal loading in the form of cyclic histories of temperatures applied to appropriate nodes of the BOPACE structural model. In addition, cyclic forces due to combustion gas pressure and coolant pressure were accounted for. Output from BOPACE provided histories of stress and strain components and their effective values (i.e., equivalent uniaxial values) for the complete thermal and mechanical loading cycle.

Structural Analysis Model

The finite element model used for the structural analysis is shown in figure 21. This model represented a three-dimensional sector taken from the throat region of the cylinder where the thermal loading was the most severe. Because of symmetry of geometry and loading conditions at the cylinder throat region, it was possible to perform the structural analysis with a model bounded by the inner and outer surfaces and by sliding boundary radial planes through the center of the channel ribs and coolant channels. One of the surfaces that bounded the model in the axial direction was fixed while the other was free to move axially thus representing a free ended cylinder condition.

A nine element model was selected based on the model study performed in reference 14. It was found that a three-dimensional model composed of nine elements produced results that compared favorably with those obtained from a two-dimensional model composed of 281 constant-strain triangle elements. Gauss integration points located within each element and near each corner node provided for output in the form of stresses and strains at those locations for each increment of loading during the cycle.

Input data used to characterize the temperature dependent nonlinear material properties were developed from the data of reference 15. The contribution of the relatively thin coating to the structural strength of the cylinders is insignificant and therefore was not included in the model for the coated cylinders. The coating, of course, had a significant effect on lowering the copper liner hot-gas-side metal wall temperature and hence the temperature difference between the copper liner hot gas-side-wall and the backside wall. A reduction in these parameters significantly affects the cyclic strain range and hence life. Therefore, the structural analyses of the coated and uncoated cylinders employed the same model with different temperature profiles and different liner materials. Wrought annealed OFHC copper properties were used for the uncoated cylinder liner and electroformed copper properties were used for the coated cylinder liners.

Structural Analysis Results

It was pointed out earlier that cylinder S/N 37 initially had a 0.203 mm (0.008 in.) coating that partially eroded away to a stabilized thickness of 0.061 mm (0.0024 in.). For the structural analysis, these two conditions were treated as two cylinders with different coating thicknesses. That is, it was assumed that one cylinder had an initial coating of 0.203 mm (0.008 in.) and the other had an initial coating of 0.061 mm (0.0024 in.) and that these coatings remained at these thicknesses throughout the theoretical lives of the cylinders. Therefore, in the following discussion reference is made to three cylinders, one uncoated cylinder and two cylinders with coating thicknesses of 0.203 mm (0.008 in.) and 0.061 mm (0.0024 in.), respectively.

Figure 22 shows the cyclic effective strain on the hot-gas-side wall at the rib centerline as a function of cycle time. The maximum effective strain occurred at this location for each of the three cylinders. It can be seen that the maximum effective strain for each cylinder occurred at approximately 0.3 second after ignition defined as zero on the time scale. The minimum effective strain occurred at approximately 2.2 seconds after ignition for the uncoated cylinder and the cylinder with the 0.061 mm (0.0024 in.) coating and at approximately 2.0 seconds after ignition for the cylinder with the 0.203 mm (0.008 in.) coating. These were the times when the maximum temperature difference between the hot-gas-side metal wall and the backside wall occurred. The maximum effective strain for the cylinder with the 0.061 mm (0.0024 in.) coating was approximately one-half that of the uncoated cylinder and the maximum effective strain for the cylinder with the 0.203 mm (0.008 in.) coating was approximately one-twelfth that of the uncoated cylinder. This, of course, was attributed to the lower hot-gas-side metal wall temperature that the coating provided.

Since effective strain is always a positive quantity, it was necessary to study the mechanical component strains to determine if any strain reversal occurred during the cycle. Figure 23 shows the mechanical component strains for the cylinder with the 0.061 mm (0.0024 in.) coating. The radial strain was continuously positive and the circumferential and axial strains were continuously negative during the entire cycle. This behavior was typical of the mechanical component strains for the three cylinders. Therefore, the strain ranges for life prediction were taken as the difference between the maximum and minimum effective strains. If strain reversal had occurred, these quantities would have been added.

Figure 24 shows the effective strain range distribution at the throat plane for the three cylinders. The maximum strain range occurred on the hot-gas-side wall at the rib centerline for the uncoated cylinder and the cylinder with the 0.061 mm (0.0024 in.) coating and on the hot-gas-side wall at the cooling passage centerline for the cylinder with the 0.203 mm (0.008 in.) coating. Using these maximum strain ranges and the material life curves of figure 25 taken from reference 16, the theoretical lives of the uncoated cylinder and the cylinder with the 0.061 mm (0.0024 in.) coating were found to be 300 cycles and 1900 cycles, respectively. Because of the small strain range obtained for the cylinder with the 0.203 mm (0.008 in.) coating, it was only possible to conclude from figure 25 that the theoretical life of this cylinder is greater than 10 000 cycles.

Concluding Remarks

The 0.203 mm (0.008 in.) coating, although a very effective thermal barrier, appeared to be too thick as evidenced by the erosion that took place during the cyclic testing. The fact that the eroded coating thickness stabilized at 0.061 mm (0.0024 in.) suggests that if the coating had been that thickness initially possibly no erosion would have taken place. However, at the present time, there is no evidence to substantiate this. Although erosion of the coating occurred, the remaining coating was well adhered. Hence, electroforming a metal wall to a relatively rough ceramic appears to provide better adhesion than the conventional method of spraying the ceramic coating onto a smooth wall.

Due to the profound reduction in effective strain and the accompanying large potential increase in life that can be achieved by use of ceramic coatings, the further development of reliable coating systems for rocket thrust chamber application appears to be a worthwhile endeavor.

Summary of Results

Two cylindrical rocket thrust chamber cylinders were coated with 0.203 mm (0.008 in.) of zirconium-oxide and cyclically tested to show the effect of the coating on thrust chamber life. The tests were conducted at a nominal chamber pressure of 4.14 MN/m^2 (600 psia) using hydrogen-oxygen propellants at an oxidant-fuel ratio of 6.0. The

cylinders were cooled with liquid hydrogen at an average flow rate of 1.0 kg/sec (2.2 lbm/sec). Although neither of the coated cylinders achieved their theoretical expected lives, due to causes unrelated to the coating system, the following results were obtained:

1. One coated cylinder endured 659 thermal cycles, despite a blocked cooling passage, as compared with 210 cycles for an uncoated cylinder tested at the same conditions.

2. In the regions of the cylinders where the coating eroded, the original 0.203 mm (0.008 in.) coating eroded to a stabilized thickness of 0.061 mm (0.0024 in.) in the first 80 cycles.

3. Excluding the local burnout area on one cylinder, there was no other area on either cylinder where the copper wall was exposed due to failure of the coating to adhere.

4. The coatings had a significant effect on suppressing the characteristic cooling passage wall deformation and thinning observed on previously tested uncoated cylinders.

5. The calculated hot-gas-side metal wall temperature, the hot-gas-side to backside metal wall temperature difference, and the heat flux were reduced approximately 80 percent where the coating was 0.203 mm (0.008 in.) thick and 40 percent where the coating was 0.061 mm (0.0024 in.) thick when compared to the uncoated cylinder.

6. The 0.203 mm (0.008 in.) coating and the remaining 0.061 mm (0.0024 in.) coating reduced the theoretical maximum effective strain in the cooling passage wall to one-twelfth and one-half that of the uncoated cylinder, respectively.

7. The reduced strains showed the theoretical lives of coated cylinders to be greater than 10 000 cycles for a stable 0.203 mm (0.008 in.) coating and 1900 cycles for a stable 0.061 mm (0.0024 in.) coating, compared to a predicted 300 cycle life for an uncoated cylinder.

References

1. Quentmeyer, R. J., "Experimental Fatigue Life Investigation of Cylindrical Thrust Chambers," AIAA Paper 77-893, July 1977.

2. Hannum, N. P., Kasper, H. J., and Pavli, A. J., "Experimental and Theoretical Investigation of Fatigue Life in Reusable Rocket Thrust Chambers," AIAA Paper 76-685, July 1976.

3. Fulton, D., "Investigation of Thermal Fatigue in Non-Tubular Regeneratively Cooled Thrust Chambers, Volume 2," Rockwell International Corp., Canoga Park, Calif., R-9093-Vol-2, May 1973 (AD-760583; AFRPL-TR-73-10-Vol-2).

4. Price, H. G., Jr., Schacht, R. L., and Quentmeyer, R. J., "Reliability and Effective Thermal Conductivity of Three Metallic-Ceramic Composite Insulating Coatings on Cooled Hydrogen-Oxygen Rockets," NASA TN D-7392, 1973.

5. Schacht, R. L., Price, H. G., Jr., and Quentmeyer, R. J., "Effective Thermal Conductivities of Four Metal-Ceramic Composite Coatings in Hydrogen-Oxygen Rocket Firings," NASA TN D-7055, 1972.

6. Curren, A. N., Grisaffe, S. J., and Wycoff, K. C., "Hydrogen Plasma Tests of Some Insulating Coating Systems for the Nuclear Rocket Thrust Chamber," NASA TM X-2461, 1972.

7. Stubbs, V. R., "Development of a Thermal Barrier Coating for Use on a Water-Cooled Nozzle of a Solid Propellant Rocket Motor," Aerojet-General Corp., Sacramento, CA, May 3, 1969. (NASA CR-72549)

8. Lewis, W. J., "Coatings for Regenerative Engines," Rep. 28238T-FR-1, Aerojet-General Corp., Sacramento, CA, July 12, 1968. (NASA CR-72413)

9. Lewis, W. J., "Coatings for Advanced Thrust Chambers," Aerojet-General Corp., El Monte, CA, 1968. (NASA CR-72604)

10. Hjelm, L. N., and Bornhorst, B. R., "Development of Improved Ceramic Coatings to Increase the Life of XLR 99 Thrust Chamber," NASA TM X-57072, 1961, pp. 227-253.

11. Hammer, S., and Czacka, Z., "Development of Advanced Fabrication Techniques for Regeneratively Cooled Thrust Chambers by the Electroforming Process," Camin Labs., Inc., Brooklyn, N.Y., Oct. 1, 1968. (NASA CR-72698)

12. Smith, J. P., "Systems Improved Numerical Differencing Analyzer (SINDA): User's Manual," TRW Systems Group, Redondo Beach, Calif., TRW-14690-H001-RO-00, Apr. 1971.

13. Vos, R. G., and Straayer, J. W., "BOPACE-3D (Boeing Plastic Analysis Capability for 3-Dimensional Solids Using Isoparametric Finite Elements)," Boeing Aerospace Co., Seattle, WA, D180-18677-1, Apr. 1975. (NASA CR-143891)

14. Armstrong, W. H., and Brogren, E. W., "3-D Thrust Chamber Life Prediction," Boeing Aerospace Co., Seattle, WA, Mar. 1976. (NASA CR-134979)

15. Esposito, J. J., and Zabora, R. F., "Thrust Chamber Life Prediction. Volume I: Mechanical and Physical Properties of High Performance Rocket Nozzle Materials," Boeing Aerospace Co., Seattle, WA, D180-18673-1-Vol-1, Mar. 1975. (NASA CR-134806)

16. Conway, J. B., Stentz, R. H., and Berling, J. T., "High Temperature, Low-Cycle Fatigue of Copper-Base Alloys in Argon. Part I: Preliminary Results for 12 Alloys at 1000° F (538° C)," Mar-Test Inc., Cincinnati, OH, Jan. 1973. (NASA CR-121259)

TABLE I. - CYLINDER CONFIGURATIONS AND TEST RESULTS

Cylinder S/N	Configuration	Test cycles	Remarks
[a]34	Uncoated	210	Typical failure, crack in cooling passage wall in throat region
36	ZrO_2 coating	80	Unrepairable crack in manifold weld seam near injector, testing terminated
37	ZrO_2 coating	659	Burnout in throat region due to blocked cooling passage

[a]Results taken from ref. 1.

TABLE II. - RESULTS OF THERMAL ANALYSIS

T_{gw}, hot-gas-side coating temperature; T_{mw}, hot-gas-side metal wall temperature; ΔT, hot-gas-side metal wall to backside wall temperature difference; q, heat flux.

Cylinder S/N	Coating thickness, mm (in.)	T_{gw}, K (^{o}R)	T_{mw}, K (^{o}R)	ΔT, K (^{o}R)	q, MN/m^2 ($Btu/in^2/sec$)
34	----------	----------	844 (1520)	556 (1000)	57.2 (35)
37	0.203 (0.008)	2922 (5260)	157 (282)	90 (162)	12 (7.3)
37	0.061 (0.0024)	1878 (3380)	489 (880)	322 (580)	34 (21)

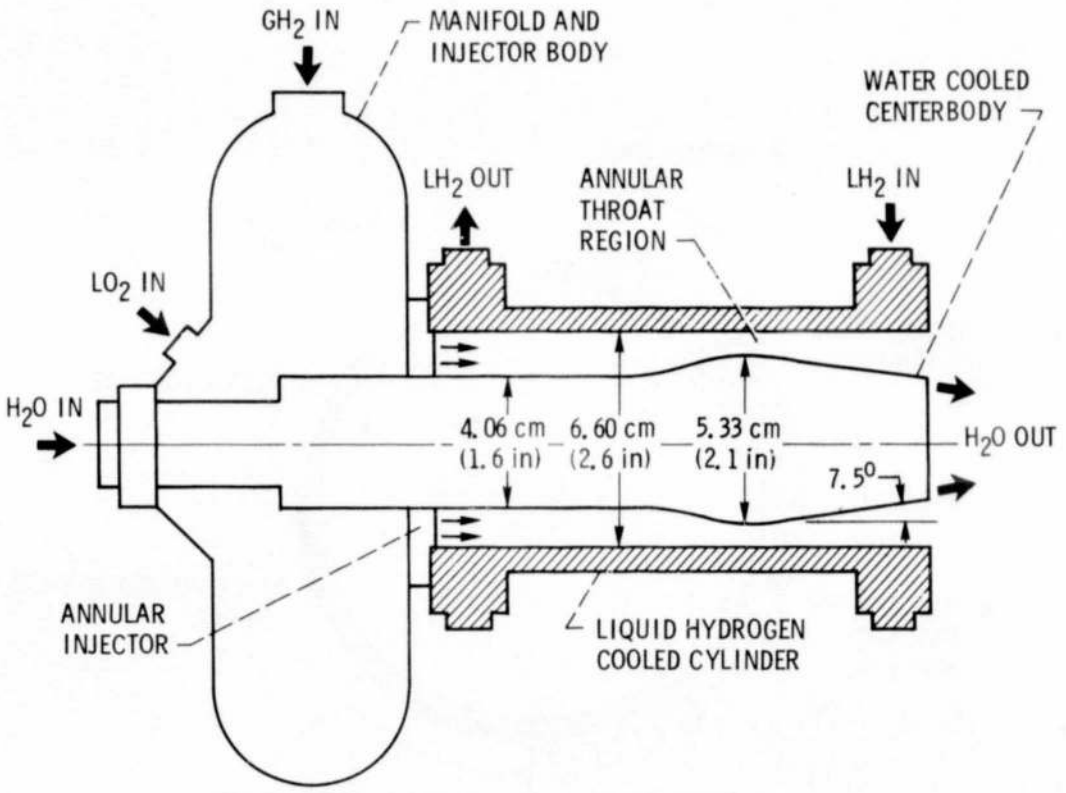

Figure 1. - Schematic of cylindrical thrust chamber assembly.

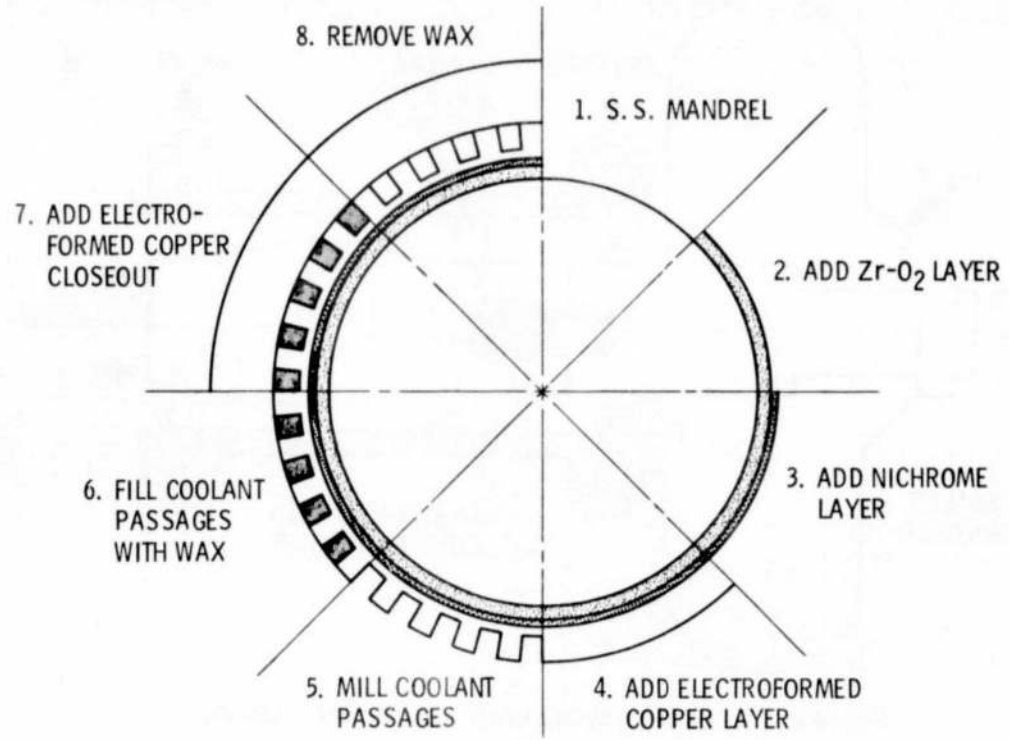

Figure 2. - Fabrication sequence for coated cylinders.

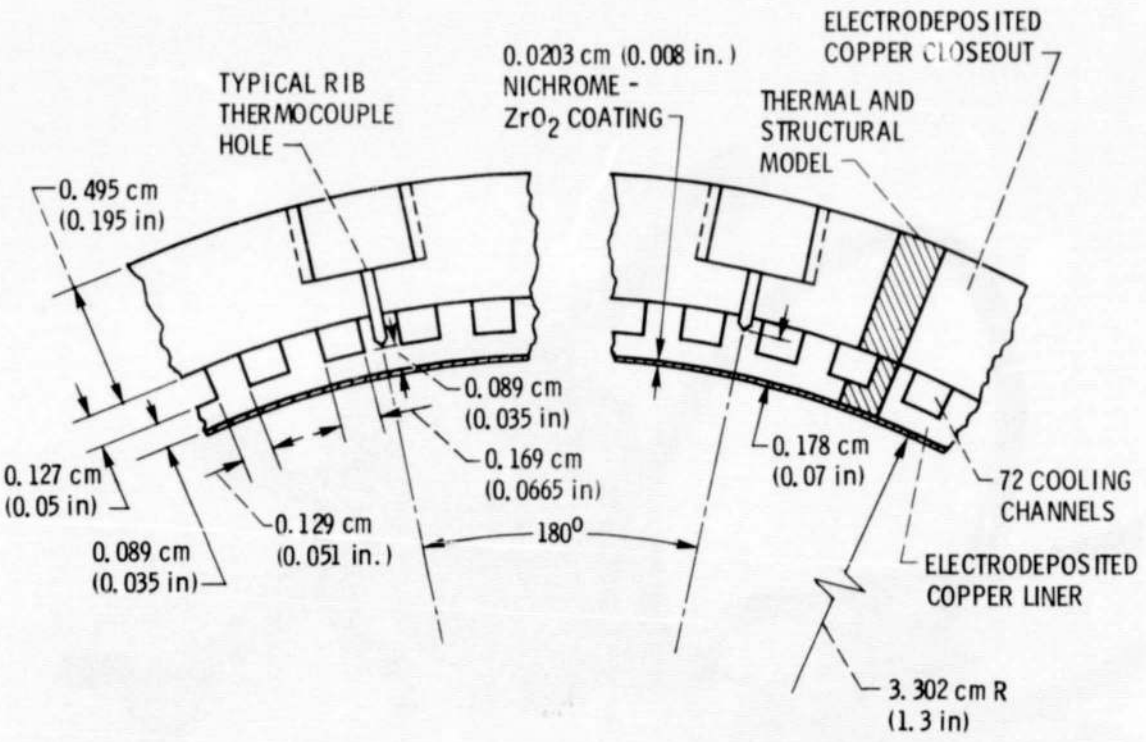

Figure 3. - Cylinder wall cross section showing instrumentation locations and dimensions.

E-2630

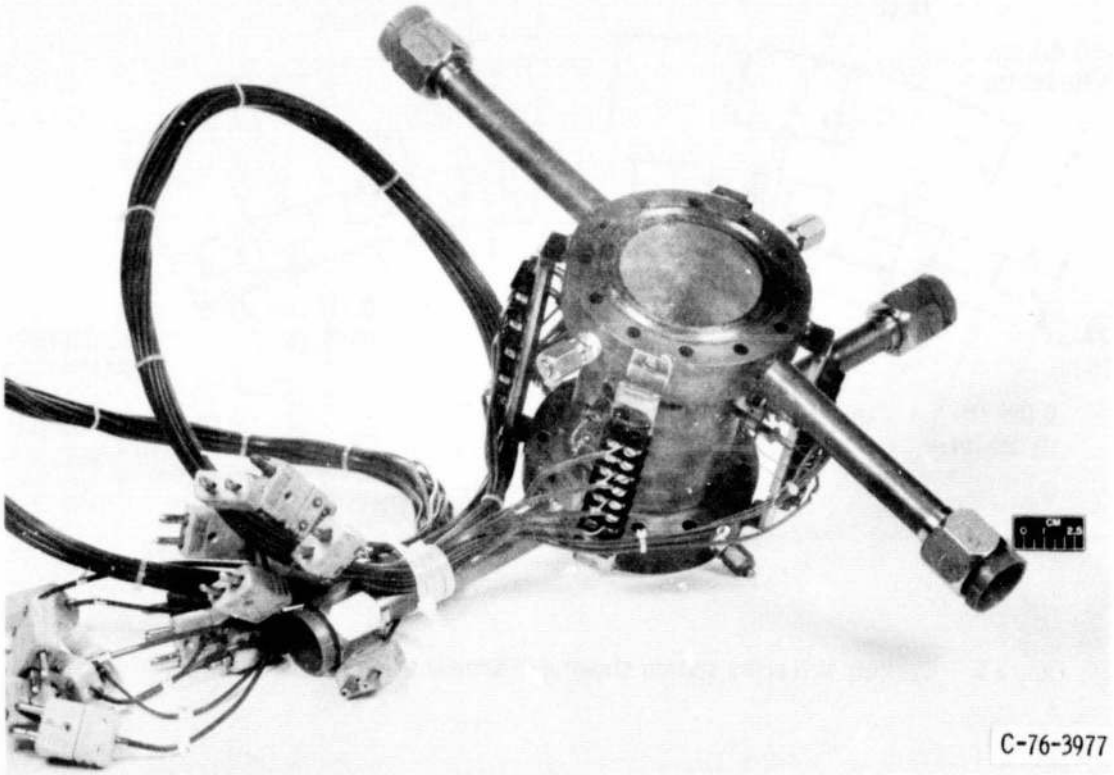

Figure 4. - Coated cylinder S/N 37 with instrumentation installed.

E-9630

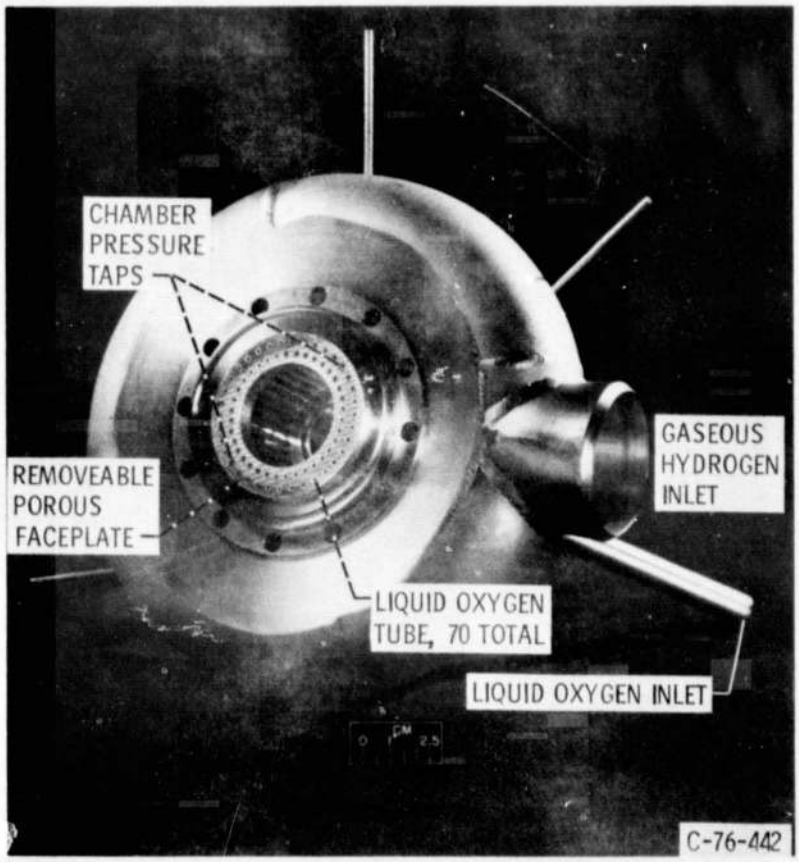

Figure 5. - Annular injector.

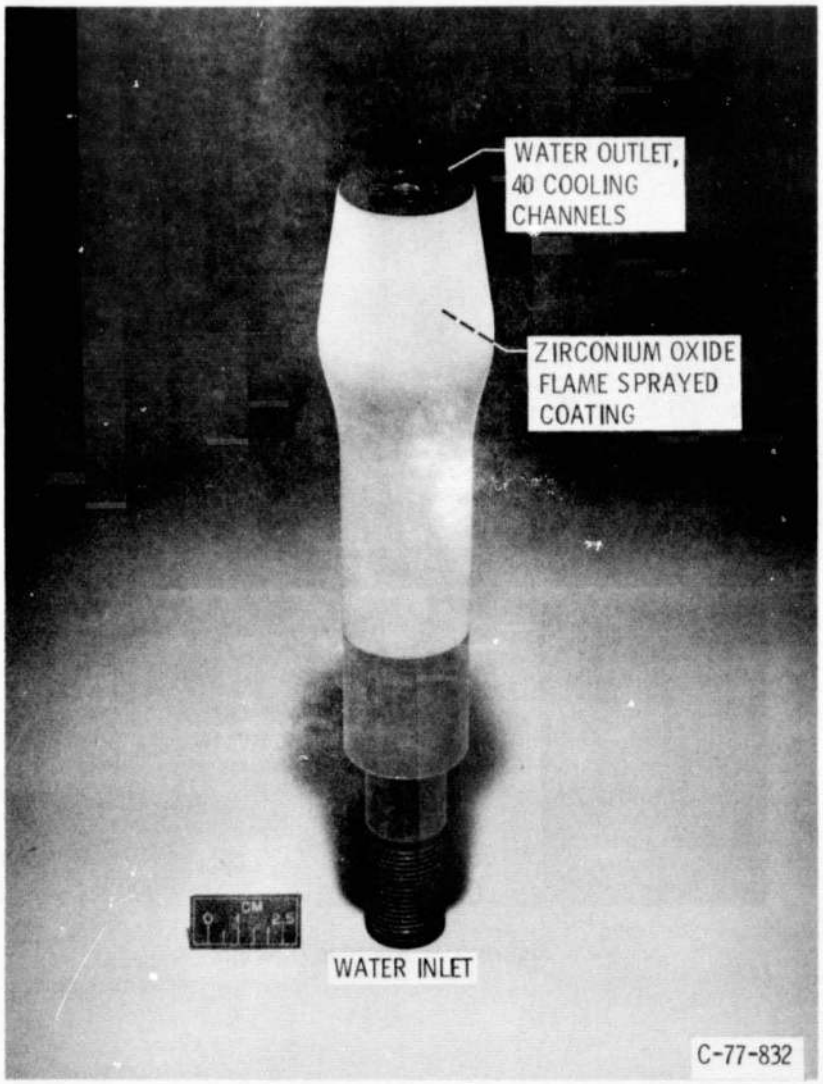

Figure 6. - Ceramic coated, water cooled centerbody for cylindrical thrust chamber.

L_1 THRUST, STRAIN-GAUGE-BRIDGE TYPE LOAD-CELL

F_1, F_2 } OXIDIZER FLOW, TURBINE TYPE FLOW METERS

P_1, P_2 } COMBUSTION CHAMBER PRESSURE, STRAIN-GAUGE-BRIDGE TYPE PRESSURE TRANSDUCER

P_3 OXIDIZER INJECTION PRESSURE, "

P_4 FUEL INJECTION PRESSURE, "

P_5 FUEL ORIFICE PRESSURE "

P_6 COOLANT OUTLET PRESSURE, "

P_7 COOLANT INLET PRESSURE, "

P_8 COOLANT TANK PRESSURE, "

P_9 WATER TANK PRESSURE, "

T_1 OXIDIZER TEMPERATURE AT FLOWMETERS, PLATINUM RESISTANCE BRIDGE TRANSDUCER

T_2 OXIDIZER INJECTION TEMPERATURE, PLATINUM RESISTANCE BRIDGE TRANSDUCER

T_3 FUEL TEMPERATURE AT ORIFICE, COPPER/CONSTANTAN THERMOCOUPLE

T_4 COOLANT TEMPERATURE AT VENTURI, PLATINUM RESISTANCE BRIDGE TRANSDUCER

T_5 COOLANT OUTLET TEMPERATURE, CHROMEL/CONSTANTAN THERMOCOUPLE

T_6 COOLANT INLET TEMPERATURE, PLATINUM RESISTANCE BRIDGE TRANSDUCER

DP_1 OXIDIZER INJECTOR PRESSURE DROP, STRAIN-GAUGE-BRIDGE TYPE PRESSURE TRANSDUCER

DP_2 FUEL INJECTOR PRESSURE DROP, "

DP_3 FUEL ORIFICE PRESSURE DROP, "

DP_4 COOLANT JACKET PRESSURE DROP, "

DP_5 COOLANT VENTURI PRESSURE DROP, "

DP_6 WATER VENTURI PRESSURE DROP, "

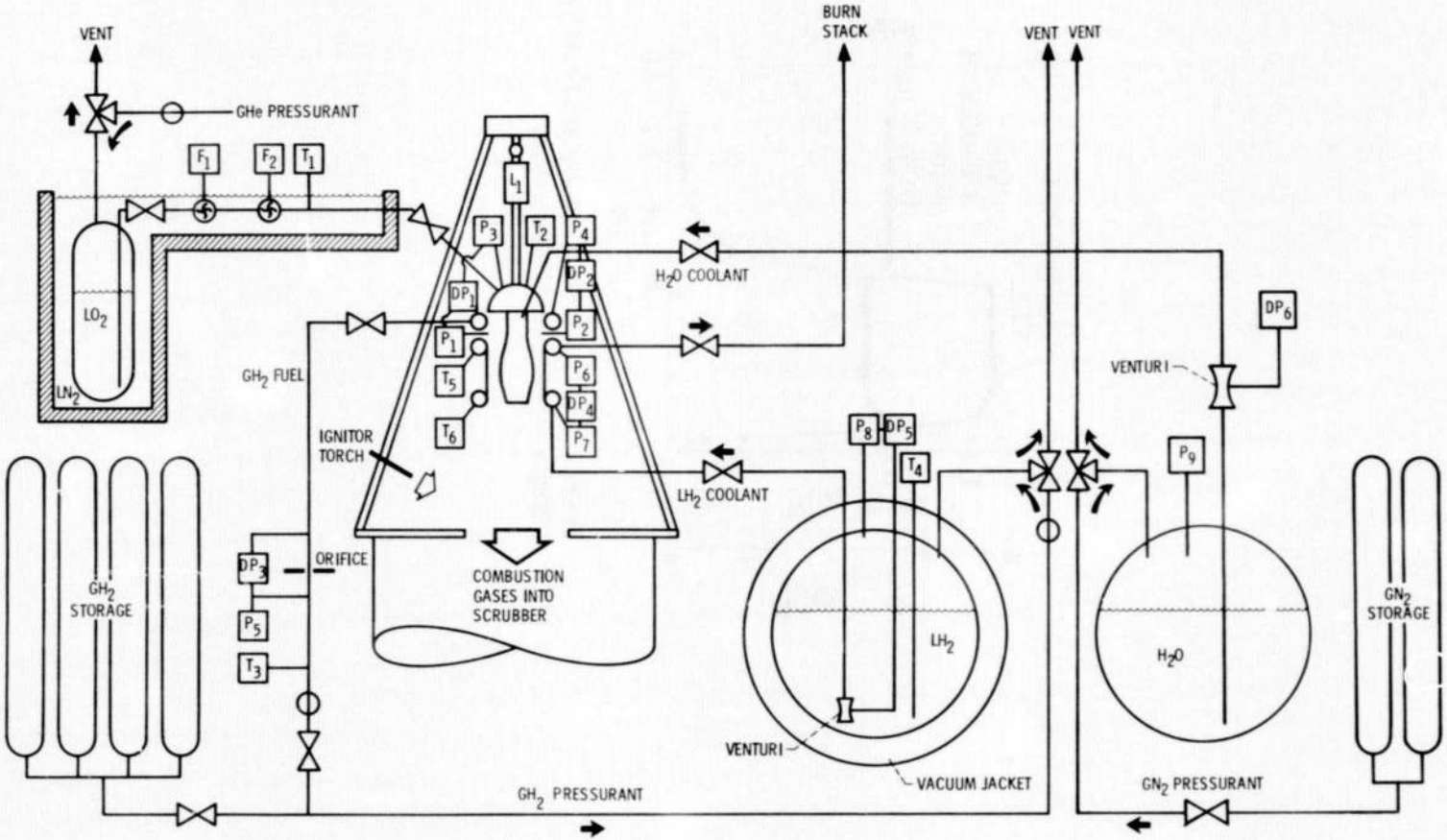

Figure 7. - Schematic of test facility.

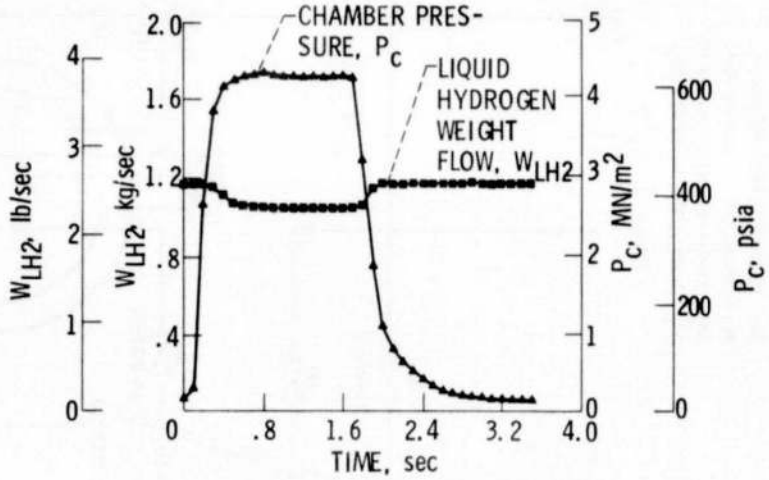

Figure 8. - Computer plot of chamber and liquid hydrogen weight flow for a typical cycle.

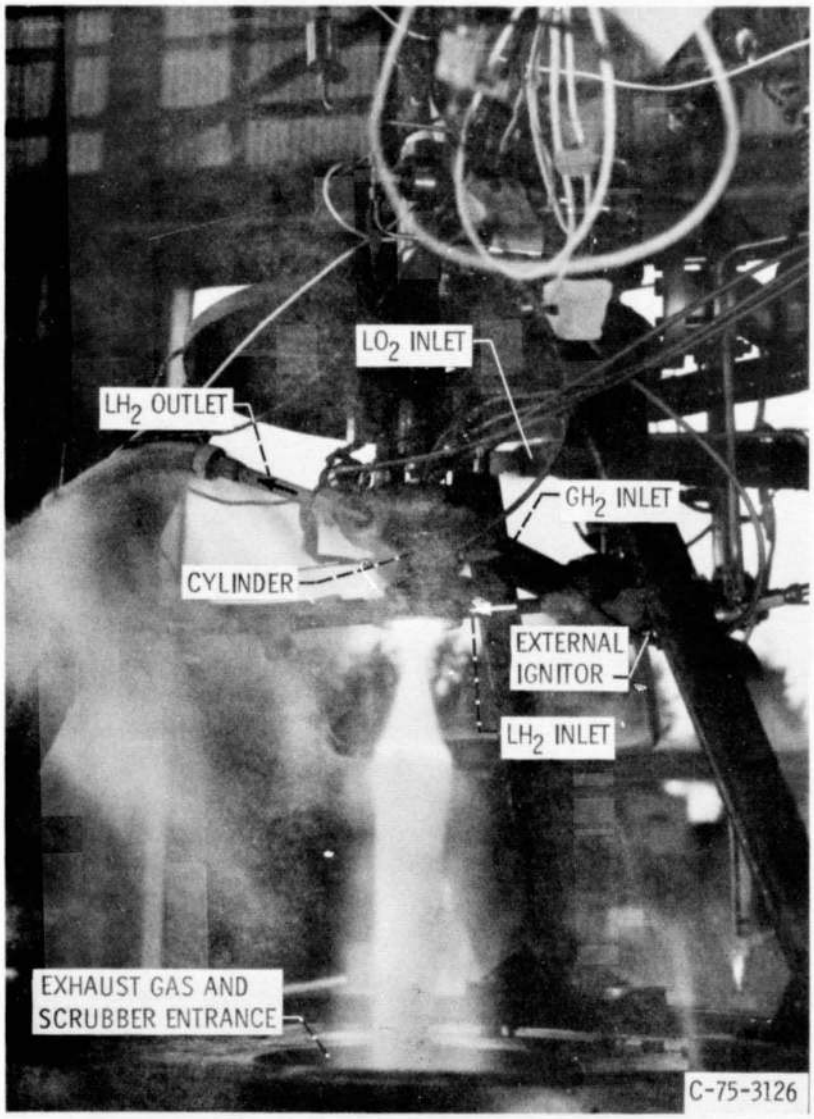

Figure 9. - Cylindrical thrust chamber during cyclic test.

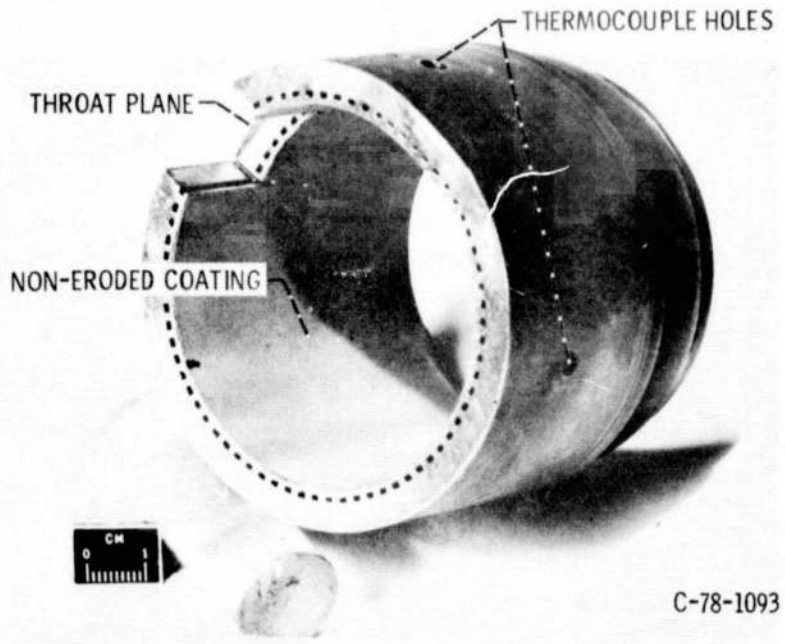

Figure 10. - Non-eroded coating in the throat region of cylinder S/N 36.

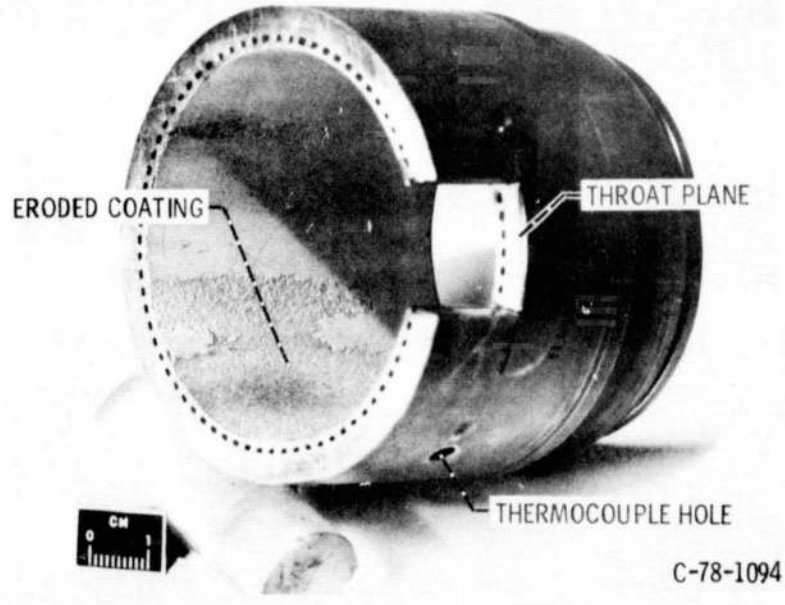

Figure 11. - Eroded coating in the throat region of cylinder S/N 36.

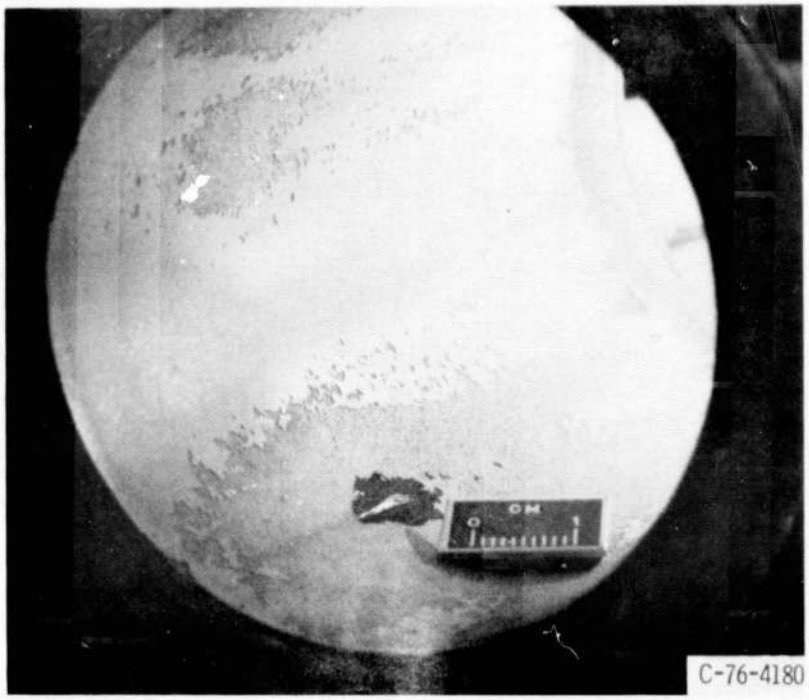

Figure 12. - Burned out cooling passage in throat region of cylinder S/N 37.

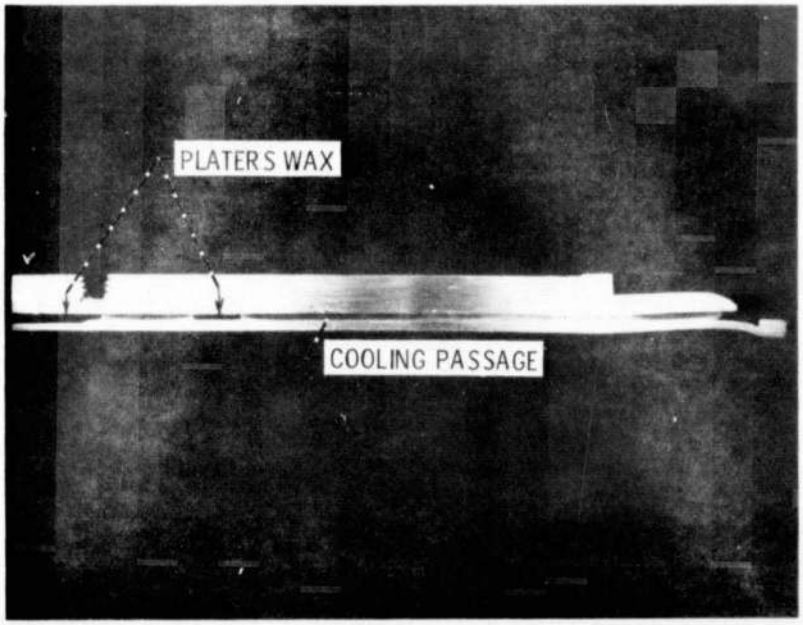

Figure 13. - Blocked cooling passage of cylinder S/N 37.

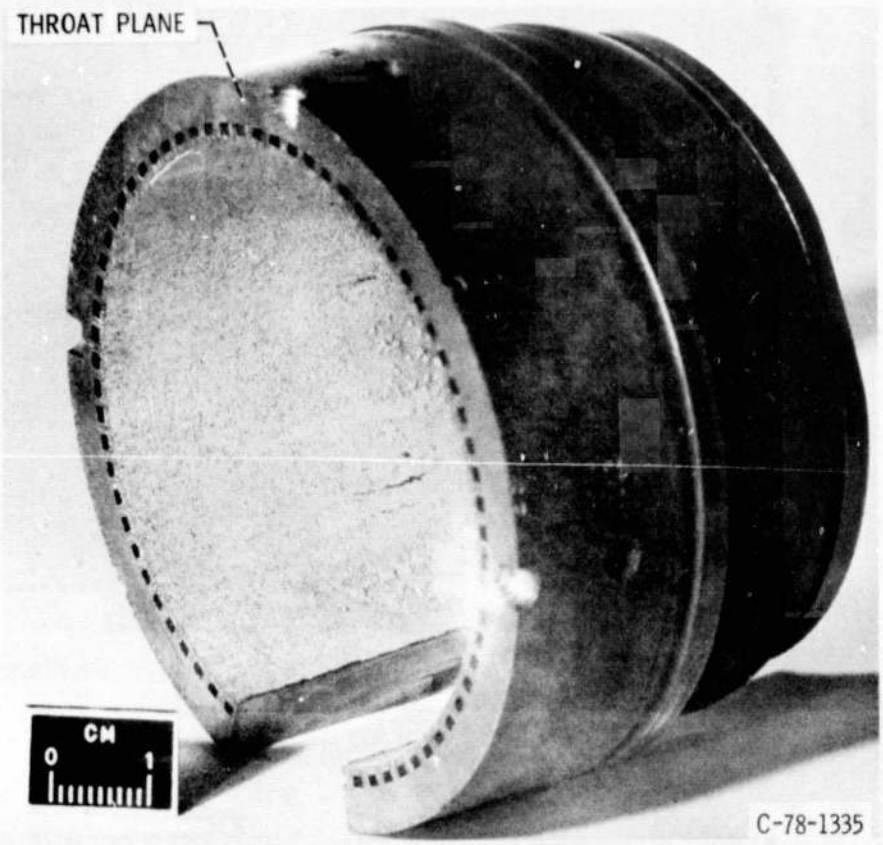

Figure 14. - Uniformly eroded coating surface of cylinder S/N 37.

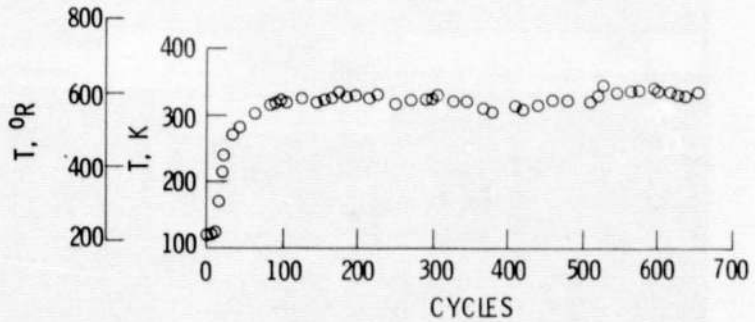

Figure 15. - Steady-state temperature of a rib thermocouple in an eroded region of coated cylinder S/N 37.

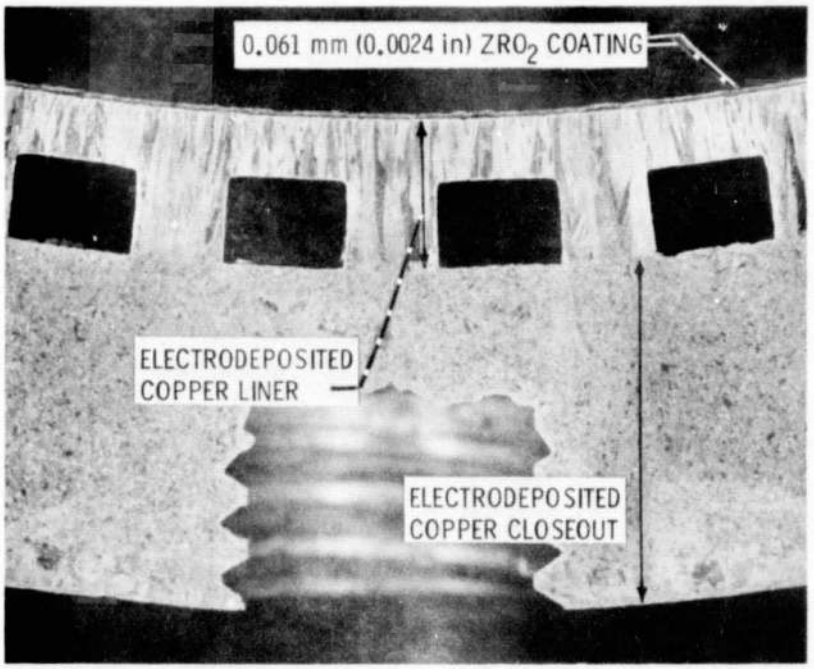

Figure 16. - Cooling passages at throat plane of cylinder S/N 37 after 659 cycles.

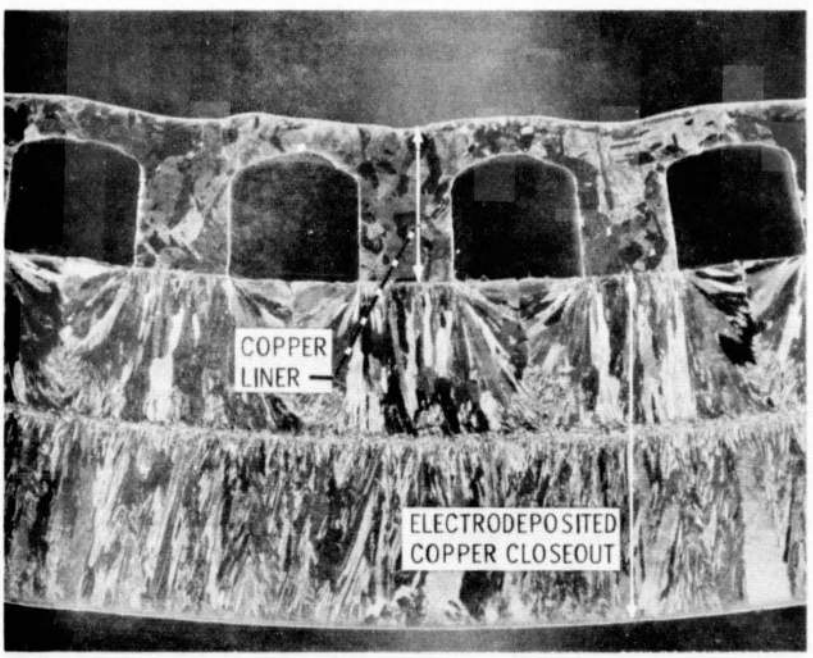

Figure 17. - Deformed cooling passages at throat plane of cylinder S/N 34 after 210 cycles.

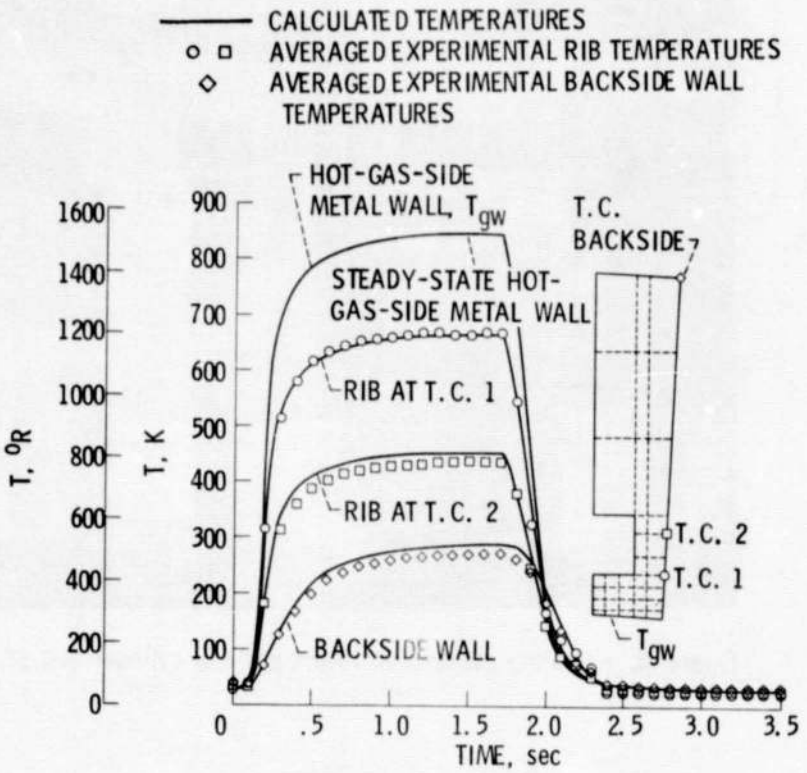

Figure 18. - Matching of thermal analysis with experimental temperature measurements of uncoated cylinder S/N 34.

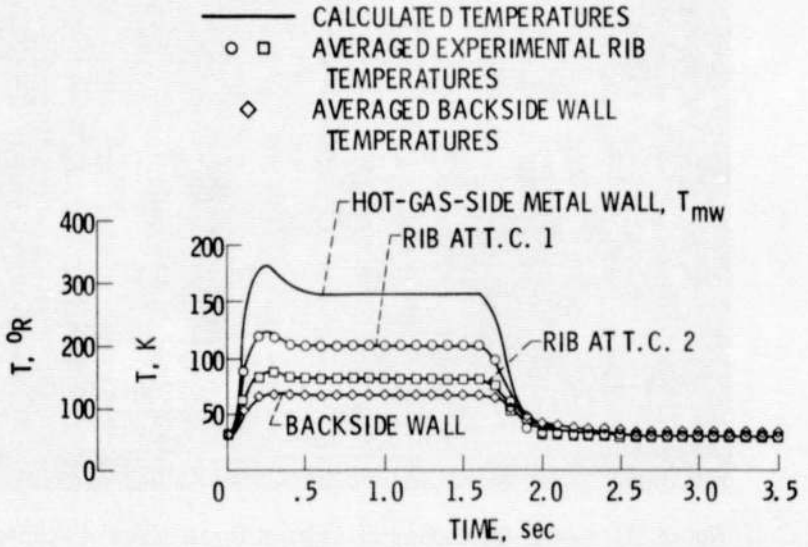

Figure 19. - Matching of thermal analysis with experimental temperature measurements of coated cylinder S/N 37.

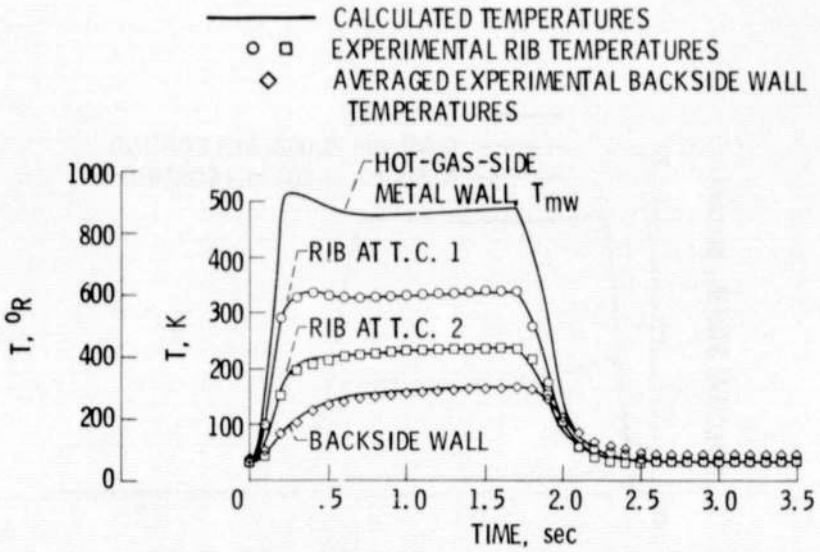

Figure 20. - Matching of thermal analysis with experimental temperature measurements for the eroded coating area of cylinder S/N 37.

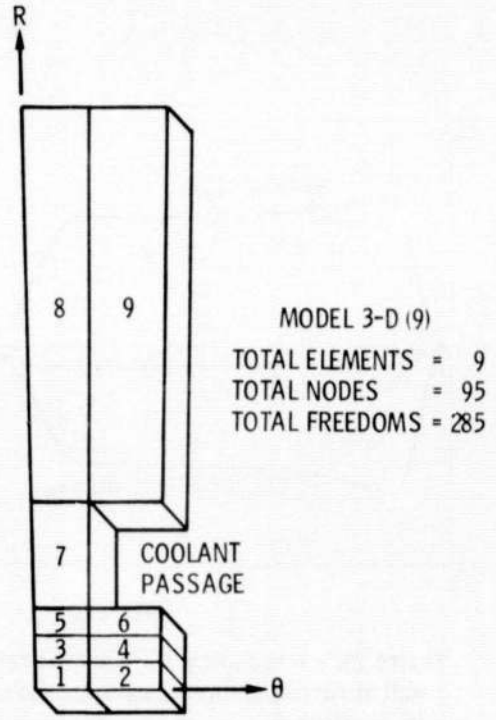

Figure 21. - Bopace 3-D finite element model.

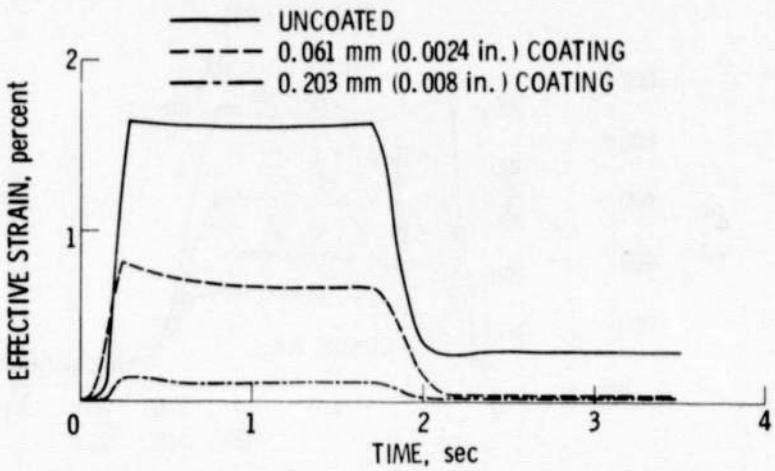

Figure 22. - Cyclic effective strain on hot gas side wall at rib centerline.

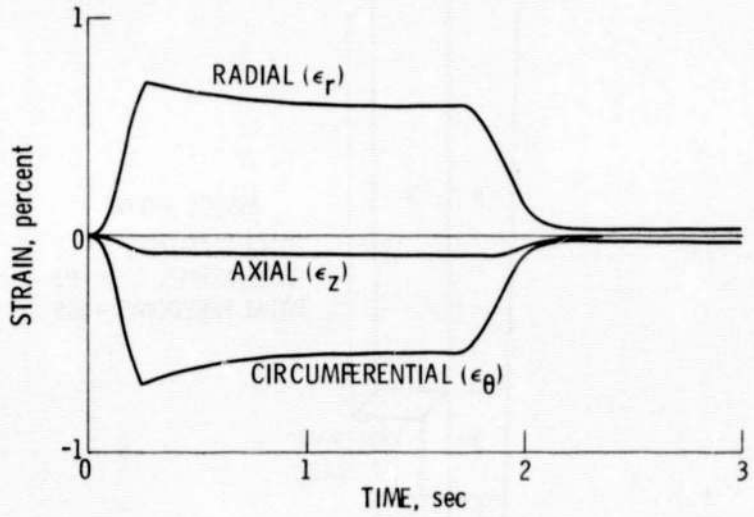

Figure 23. - Mechanical component strains on hot gas side wall at rib centerline for cylinder with 0.061 mm (0.0024 in.) coating.

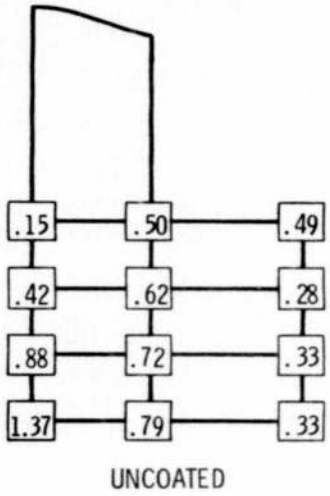

UNCOATED

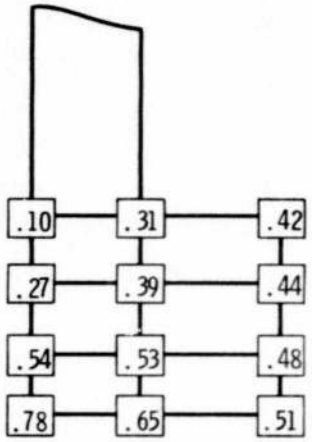

0.061 mm (0.0024 in.)
COATING

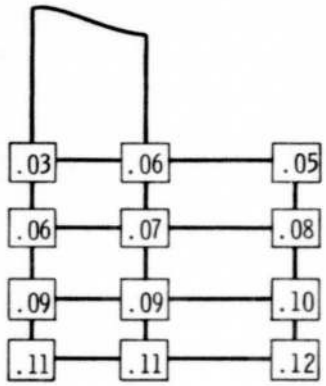

0.203 mm (0.008 in.)
COATING

Figure 24. - Effective strain range distribution (percent) at cylinder throat plane for three cylinders.

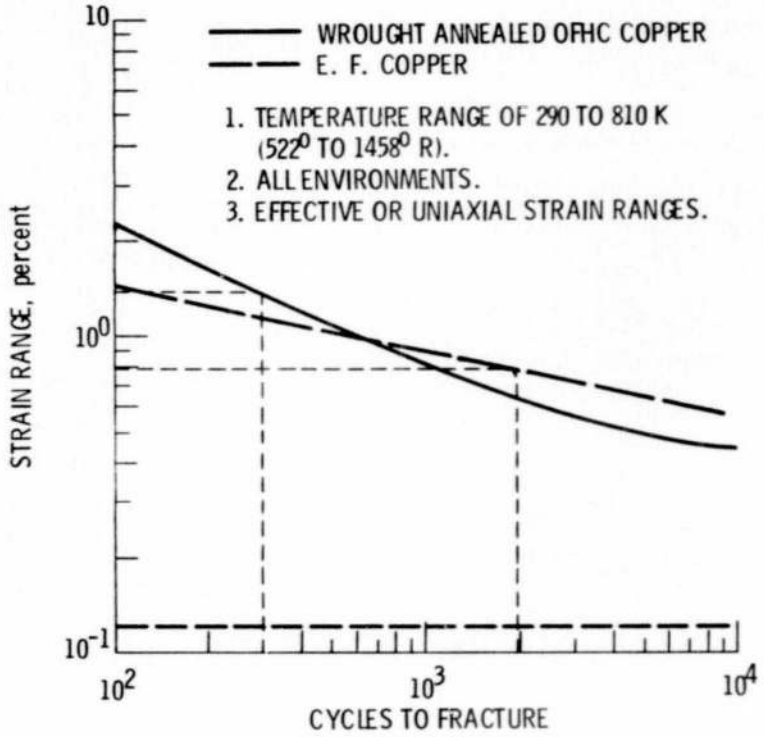

Figure 25. - Typical low-cycle fatigue life of wrought annealed OFHC copper and electroformed copper (E. F. Cu).